CELL BIOLOGY

Gradient bimetallic ion–based hydrogels for tissue microstructure reconstruction of tendon-to-bone insertion

Renhao Yang[1†], Gen Li[1†], Chengyu Zhuang[1†], Pei Yu[1], Tingjun Ye[1], Yin Zhang[1], Peiyang Shang[1], Jingjing Huang[1], Ming Cai[2], Lei Wang[1]*, Wenguo Cui[1]*, Lianfu Deng[1]*

Although gradients play an essential role in guiding the function of tissues, achieving synchronous regeneration of gradient tissue injuries remains a challenge. Here, a gradient bimetallic (Cu and Zn) ion–based hydrogel was first constructed via the one-step coordinative crosslinking of sulfhydryl groups with copper and zinc ions for the microstructure reconstruction of the tendon-to-bone insertion. In this bimetallic hydrogel system, zinc and copper ions could not only act as crosslinkers but also provide strong antibacterial effects and induce regenerative capacity in vitro. The capability of hydrogels in simultaneously promoting tenogenesis and osteogenesis was further verified in a rat rotator cuff tear model. It was found that the Cu/Zn gradient layer could induce considerable collagen and fibrocartilage arrangement and ingrowth at the tendon-to-bone interface. Overall, the gradient bimetallic ion–based hydrogel ensures accessibility and provides opportunities to regenerate inhomogeneous tissue with physiological complexity or interface tissue.

INTRODUCTION

Metal ions play an important role in the ordinary processes of the human body (*1*), including maintaining life functions, regulating metabolism, and promoting tissue repair (*2*). Many metal ions, such as Cu^{2+}, Ca^{2+}, and Ag^{2+}, can promote bone regeneration by balancing the function of osteoblasts and osteoclasts (*3*). Zinc ions can repair damaged skin by promoting extracellular matrix (ECM) synthesis and secretion (*4*). In different tissues, the content of those metal ions is various, and different biologically active ions have a combined or synergistic effect on tissue regeneration (*5*). The selectivity of different tissues for metal ions is particularly important. For example, bioactive glass containing copper ions can be used for bone repair, and a novel tubular scaffold containing zinc oxide nanoparticles can achieve tendon repair (*6*, *7*). Currently, in complexly damaged tissues, it is highly challenging to achieve the selective absorption of different metal ions in different tissues to promote the synchronous reconstruction and regeneration of damaged tissues.

Gradients play essential roles in guiding the functions of a wide range of tissues, including the tendon-to-bone interface in the rotator cuff. Clinically, rotator cuff injury is the most common cause of shoulder joint disease, mainly due to poor healing of the tendon-to-bone interface after surgery (*8*, *9*). The normal morphology of the tendon-to-bone interface evolves layer by layer, including gradual changes in mineral content, staggered arrangement of collagen fibers, and compliant matrix tissue thickening (*10*–*13*). A strategy to recreate these natural gradients has been developed in the field of tissue engineering (*14*). However, owing to the complex structure of gradients in human tissues, it is difficult to balance the growth of various tissue types, resulting in scar tissue formation (*14*). Therefore, it is difficult to achieve complete regeneration of the tendon-to-bone interface (*15*, *16*). The tissue engineering materials used for the treatment of rotator cuff tear (RCT) mainly include regenerated scaffolds, such as oriented collagen fiber braids, poly-l-lactic acid (PLLA) scaffolds, layered decellularized matrix scaffolds, and allografts (*17*–*21*). However, some deficiencies remain, such as insufficient release time, complicated preparation process, and poor biocompatibility of these materials. Furthermore, regeneration-induced tissues cannot achieve synchronous regeneration, leading to disordered rotator cuff tissue formation after repair and poor biomechanical functionalities (*22*). Therefore, further information on the construction of materials with layered gradient structures and the repair capability is particularly necessary in the field of tissue microstructure. In the early stage, we used a bipolar electrospinning nanofiber membrane. The upper layer comprised a poly-L-lactic acid (PLLA) fiber membrane, and the lower layer included the PLLA fiber membrane loaded with nano-hydroxyapatite to promote the simultaneous regeneration of bone and tendon and achieve the healing of the tendon-to-bone interface (*23*). However, the tissues that release inorganic ions in the fibrous membrane showed poor biocompatibility, which led to fibrosis at the tendon-to-bone interface.

In the field of tissue regeneration, metal ions also play important roles. For example, copper ions can regulate the osteogenic differentiation of osteoblasts and angiogenesis, and Fe^{2+} can promote osteogenesis by promoting blood vessel growth (*24*, *25*). Different metal ions can induce the regeneration of different tissues. Therefore, on the basis of the advantages of various metal ions for tissue regeneration, designing a novel metal ion–based biomaterial is expected to regulate the overgrowth of different gradient tissues.

To achieve healing at the tendon-to-bone interface, we took advantage of the ECM-mimicking properties of gelatin hydrogel, the tissue repairing abilities of copper and zinc ions, and the excellent antibacterial ability of metal ions (*26*, *27*). In this study, a novel gradient bimetallic ion–based hydrogel, which is compatible with the

[1]Department of Orthopaedics, Shanghai Key Laboratory for Prevention and Treatment of Bone and Joint Diseases, Shanghai Institute of Traumatology and Orthopaedics, Ruijin Hospital, Shanghai Jiao Tong University School of Medicine, 197 Ruijin 2nd Road, Shanghai 200025, P. R. China. [2]Department of Orthopaedics, Shanghai Tenth People's Hospital, Tongji University School of Medicine, No.301 Middle Yanchang Road, Shanghai 200072, P. R. China.
*Corresponding author. Email: ray_wangs@hotmail.com (L.W.); wgcui80@hotmail.com (W.C.); lf_deng@126.com (L.D.)
†These authors contributed equally to this work.

microstructure of the tendon-to-bone insertion, was developed via the hierarchically coordinative cross-linking of thiolated gelatin with copper and zinc ions to regulate the synchronous regeneration of the microstructure (Fig. 1). In the fabrication process of the gradient bimetallic hydrogel, the upper and lower layers were covered, and free (incompletely gelled) ions in the upper layer could sink due to gravity and cross-link with free sulfhydryl groups. The sulfhydryl group and metal ions have a great dynamic cross-linking capacity, so the relatively stable dynamic gradient of the two kinds of metal ions in the bimetal hydrogel would be built after gelation (Fig. 1A).

Through planting the gradient material in vivo, the bone-tendon interface containing naturally physiological gradients such as fibrocartilage, the repairability, and regeneratibility was guaranteed (Fig. 1, B and C). This newly developed bimetallic hydrogel was proven to have a typical porous structure, good mechanical properties, and self-healing characters through material characterizations. In in vitro experiments, on the basis of the slow release of copper and zinc ions, this hydrogel was found to be functional, promoted antibacterial activity, and had an inductive effect on bone or tendon tissue, respectively. Furthermore, the gradient regeneration effect of hydrogels in vivo was detected in a rat RCT model by observing indicators, such as gross photos, imaging diagnosis, biomechanics, and histological staining. Therefore, this innovative gradient bimetallic metal ion hydrogel has a widespread applicability and provides opportunities to generate gradient interfacial tissues for microstructure reconstruction, such as RCT.

RESULTS

Characterization of hydrogels

Gelatin is one type of protein produced by the partial hydrolysis of native collagen, with excellent properties in terms of biodegradability, biocompatibility, cell adhesion features, and ease of modification (*28*). In this research, the $-NH_2$ group in gelatin reacted with Traut's reagent to form the thiolate gelatin (s-gelatin). The gelling process of s-gelatin without cross-linking was also presented in fig. S1. By mixing the s-gelatin with Cu^{2+} or Zn^{2+}, ion-based hydrogels were formed in situ via S-Cu or S-Zn coordinative cross-linking (Fig. 2, A and B). Uniform porous micromorphology in which each pore communicates with each other for all groups was observed via scanning electron microscopy (SEM) (Fig. 2, C to E, and fig. S2). Then, the hydrogel with graded metal ions was sectioned along the vertical direction for characterization via energy-dispersive spectroscopy (EDS) mapping (as shown in Fig. 2F). According to the EDS mapping results, the cross-sectional area exhibited graded distribution in both copper and zinc contents. The zinc gradually decreased from the bottom layer to the top layer, whereas the copper showed an opposite trend. The trends in different days were further quantified by dividing the interface into five average small sections. As shown in Fig. 2G, the content distribution of the copper and zinc ions did not change significantly over time, suggesting the successful establishment of a gradient. Accordingly, it was necessary to determine the cross-linking mechanism of the chemical groups. As characterized by the absorption peaks around 1076 and 1630 cm^{-1} as shown in fig. S3, numerous s-Cu bonds and s-Zn bonds were formed between Cu^{2+} and Zn^{2+} with the thiol group of gelatins, which is considered the main mechanism of cross-linking in the hydrogel. The absorption peak of both ion-based hydrogels was significantly decreased at 1076 cm^{-1} and increased at 1630 cm^{-1}, indicating that metal ions were successfully combined with the thiol group in s-gelatin.

Next, to verify the mechanical properties of the ion-based hydrogels, the gelation kinetics of the hydrogels were measured by evaluating the storage modulus (G′) and the loss modulus (G″) versus

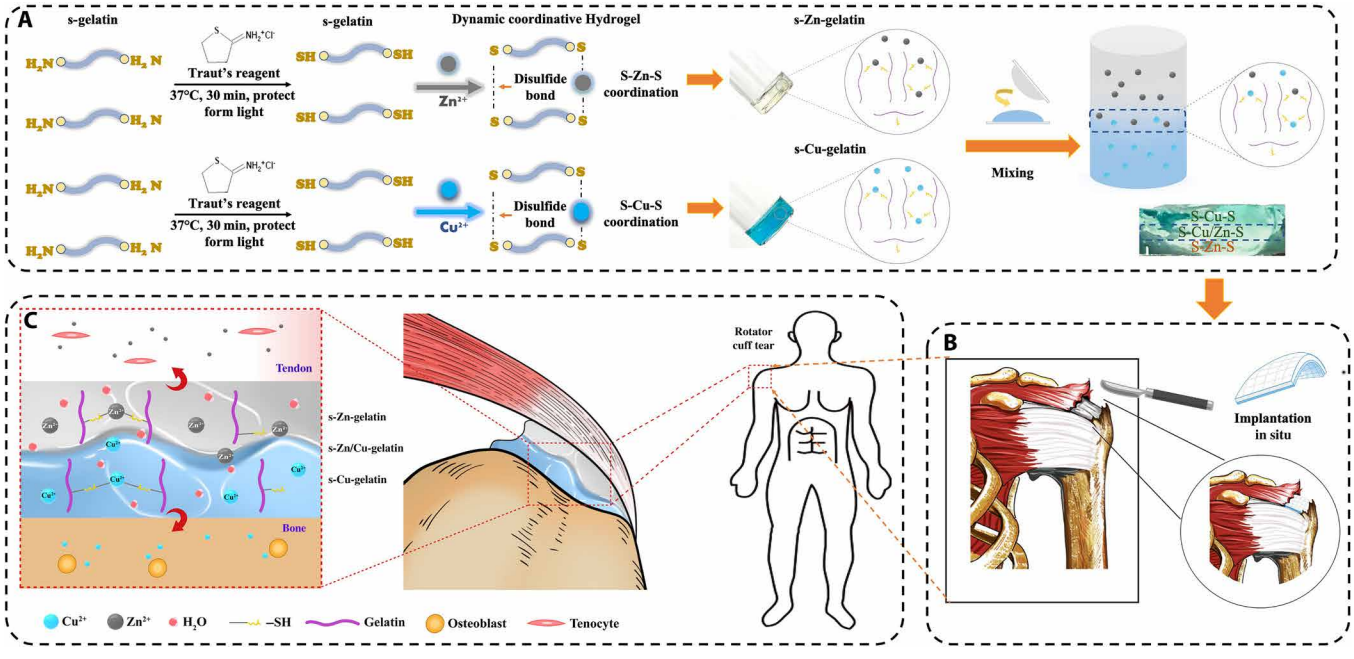

Fig. 1. The principle and fabrication of the gradient bimetallic ion–based hydrogels and the operation diagram. (**A**) The principle and fabrication of the novel gradient bimetallic hydrogels and the exhibition of the gradient structure. (**B**) The in situ implantation of the novel hydrogel for RCT. (**C**) The mechanism of the gradient hydrogel for synchronous regeneration in the tendon-to-bone insertion.

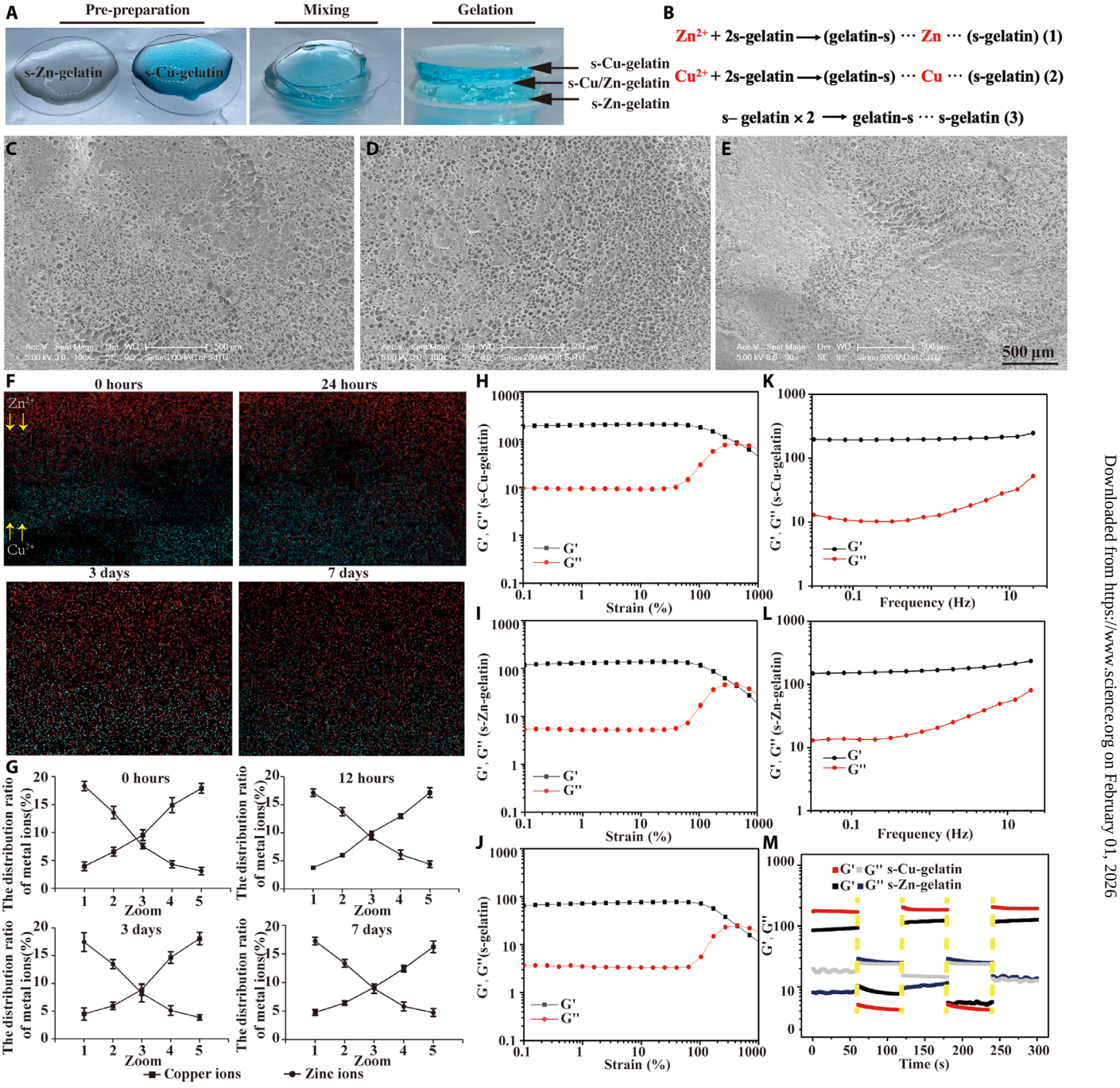

Fig. 2. The morphology and characterization of hydrogels. (**A**) Gelation process of the gradient bimetallic hydrogel. (**B**) Chemical equations of the fabrication of the s-Cu-gelatin, s-Zn-gelatin, and s-gelatin groups. (**C** to **E**) Representative SEM images of 500-μm microspheres with different groups. (**F**) EDS mapping of elemental distributions recorded from the cross section. (**G**) Quantification of copper and zinc content along the vertical direction ($n = 3$), where the x axis indicates the distance from the top to the bottom with the five average small sections. (**H** to **J**) Strain sweep measurements the s-Cu-gelatin, s-Zn-gelatin, and s-gelatin groups. (**K** to **L**) Frequency sweep measurements of the s-Cu-gelatin and s-Zn-gelatin groups. (**M**) Dynamic step–strain measurements of the s-Cu-gelatin and s-Zn-gelatin groups.

time (Fig. 2, H to J). The G′ values of both the ion-based hydrogel groups were significantly higher than those of the s-gelatin group, whereas the G″ was nearly identical among all three groups with no notable difference, as shown in fig. S4. The critical strain values that both the G′ and G″ could maintain in the solid gel and transit to the solution gel were approximately 420, 300, and 450% in the s-Cu-gelatin, s-Zn-gelatin, and s-gelatin groups, respectively. Moreover, the frequency-dependent rheological behaviors under 0.01 to 20 Hz were performed by oscillation frequency measurements (Fig. 2, K and L). It was observed that s-Cu-gelatin and s-Zn-gelatin were always in a colloidal shape, which was holding the G′ at ≈200 Pa and G′ at ≈180 Pa, respectively, in the frequency range. The results

demonstrated that s-Cu-gelatin and s-Zn-gelatin could maintain the gel condition in the frequency range of 0.01 to 20 Hz. As shown in Fig. 2M, s-Cu-gelatin and s-Zn-gelatin could maintain the gel network situation by holding the G′ at ≈200 Pa and G′ at ≈100 Pa, respectively. After high strain was subjected, the s-Cu-gelatin and s-Zn-gelatin hydrogel networks were disrupted immediately as the G′ dropped to ≈5 and ≈8 Pa, respectively. Furthermore, when transferred to the low strain, both the G′ and G″ of hydrogels recovered approximately 100% within a few seconds. This indicates that the metal ion hydrogel had the self-healing characters. To investigate the degradation capacity of hydrogels, the ion-based hydrogels were soaked in 0.15% collagenase type I solution and 1× phosphate-buffered saline (PBS) for a certain period of time (*29*, *30*). As shown in fig. S5A, regardless of the hydrogel type, all hydrogels completely degraded in 0.15% collagenase type I solution within 7 days, suggesting that this ion-based hydrogel had good biodegradability. As illustrated in fig. S5B, all hydrogels degraded gradually and remained at 20 to 30% of the initial weight after the 21st day, suggesting that this novel hydrogel had the ability to control the release of Cu^{2+} and Zn^{2+} for continuous tissue healing. Meanwhile, as the hydrogel degraded, Cu^{2+} and Zn^{2+} were gradually released into the environment and could be detected using inductively coupled plasma mass spectrometer. On the first 7 days, a rapid release trend was observed. Then, a continuous slow release was observed for the remainder of the test period. In fig. S6, the cumulative release of Zn^{2+} was 44.33 ± 5.22%, and a continuous and slow release to 74.69 ± 5.98% was observed on day 21. Meanwhile, the cumulative release of Cu^{2+} was 40.32 ± 4.23%, and the similar increase to 71.77 ± 3.83% was observed on day 21. The release and degradation behaviors revealed the same trends at the last period, suggesting that the release and degradation process were carried out simultaneously.

Biocompatibility and antibacterial property test

Specifically, in this study, the biocompatibility of ion-based hydrogels was evaluated both qualitatively and quantitatively. According to the live/dead staining results, it was obvious that the rat mesenchymal stem cells (rMSCs) could evenly distribute on these two types of hydrogel with similar morphology and cell density, as shown in Fig. 3A. Most cells maintain the spindle-like morphology after incubation for several days, and the quantified analysis of the staining results after culturing for 5 days showed good cell viability (fig. S7A), which demonstrated that the metal ion–based hydrogels had a favorable biocompatibility. Furthermore, according to the CCK8 assay results, both metal ion–based hydrogels showed no effect on proliferation compared with the control group on days 1 and 3, but a significant increase in the proliferation ability of rMSCs was observed on day 5 (Fig. 3B). Then, the biocompatibility of the novel bimetallic ion–based hydrogel was evaluated via the in situ implantation of related cells. The osteoblasts and tenocytes were seeded onto the copper ion–based hydrogels and zinc ion–based hydrogels, respectively, to evaluate the biocompatibility. According to the corresponding results of the live/dead staining results and CCK8 assays, the cells showed no statistically significant differences in cell viability and cell proliferative activity after culturing for 1, 3, and 5 days (Fig. 3, E and F). Moreover, the related quantified analysis also demonstrated the great biocompatibility of the mats (fig. S7B), and the results of flow cytometry showed that the metal ion solution (10^{-6} to 10^{-14} M) did not affect the apoptosis of the corresponding cells (figs. S8 and S9).

Zn^{2+} and Cu^{2+} have considerable antibacterial properties against Gram-positive and Gram-negative bacteria, fungi, and certain viruses, including antibiotic-resistant strains (*31*). *Staphylococcus aureus*, one of the most common pathogens, usually leads to the loosening of internal implants and unhealed wounds after orthopedic surgery (*32*, *33*). On this basis, we evaluated the antimicrobial activity of the ion-based hydrogel and pure s-gelatin. As a result, the two ion-based hydrogels showed clear antibacterial activity against *S. aureus*, but this was not observed in the s-gelatin group (Fig. 3C and fig. S10). In Fig. 3D, we carried out the Kirby-Bauer disk diffusion test and measured the diameters of a quasi-circular range of cell-free regions around the hydrogel. The diameters of s-Zn-gelatin and s-Cu-gelatin were 17.42 ± 0.87 mm and 18.53 ± 2.18 mm, respectively, and a statistically significant difference was observed between the ion-based hydrogel groups and the s-gelatin group (11.55 ± 0.87 mm). The above results suggested that this novel hydrogel system had considerable biocompatibility without cytotoxicity and could be widely used in tissue regeneration processes.

The effect on cell morphology and spreading

Cell morphology could provide a complex readout of cell state or phenotype (*34*). As shown in Fig. 4 (A and B), osteoblasts and tenocytes were seeded on the metal ion–based hydrogel. After 3 days, both kinds of cells were stained with rhodamine-conjugated phalloidin/4′,6-diamidino-2-phenylindole (DAPI), the morphology of both cells appeared to have a classical spindly-like and smooth shape, and the cell foot showed no notable change. The results indicated that the hydrogels showed no obvious influence on cell morphology.

To evaluate the effect on cell spreading, the tenocyte and osteoblasts were transfected via the lentivirus to carry the red fluorescent gene and green fluorescent gene, respectively. Then, the two transfected cells were mixed and seeded on the transition layer of the gradient bimetallic hydrogel at a ratio of 1:1 to evaluate the cell migration behavior on the hydrogel surface. After culturing for 3 days, the cell distribution showed a significant difference at the different side. The osteoblasts appeared more affinity for copper ion–based hydrogel, and the tenocytes appeared more affinity for zinc ion–based hydrogel (Fig. 4C). The cell distribution was further quantified by dividing the interface into three small parts, including the copper side, the zinc side, and the transition layer, and the correlation percentage of the cell distribution was shown in Fig. 4 (D and E). More osteoblasts were observed around the copper side, whereas more tenocytes were observed around the zinc side. At the transition surface, the distribution of the two kinds of cells was basically average and random. Furthermore, the gradient bimetallic hydrogel had a different influence on cell distribution for the corresponding cell population. Overall, the tenocytes were more suitable for growth on zinc-based hydrogels, and the osteoblasts were more suitable for growth on copper-based hydrogels.

Osteogenesis assay in vitro

To determine whether ion-based hydrogels promote osteogenic induction, we investigated the differentiation of osteoblasts cocultured with hydrogels from different groups by measuring the alkaline phosphatase (ALP) activity and ECM mineralization using ALP and Alizarin Red staining, respectively. First, we performed the early osteogenic characterization of s-Cu-gelatin via ALP staining. After culturing for 1, 3, 7, and 14 days, the ALP staining was found to gradually deepen, indicating that the degree of mineralization and osteogenic

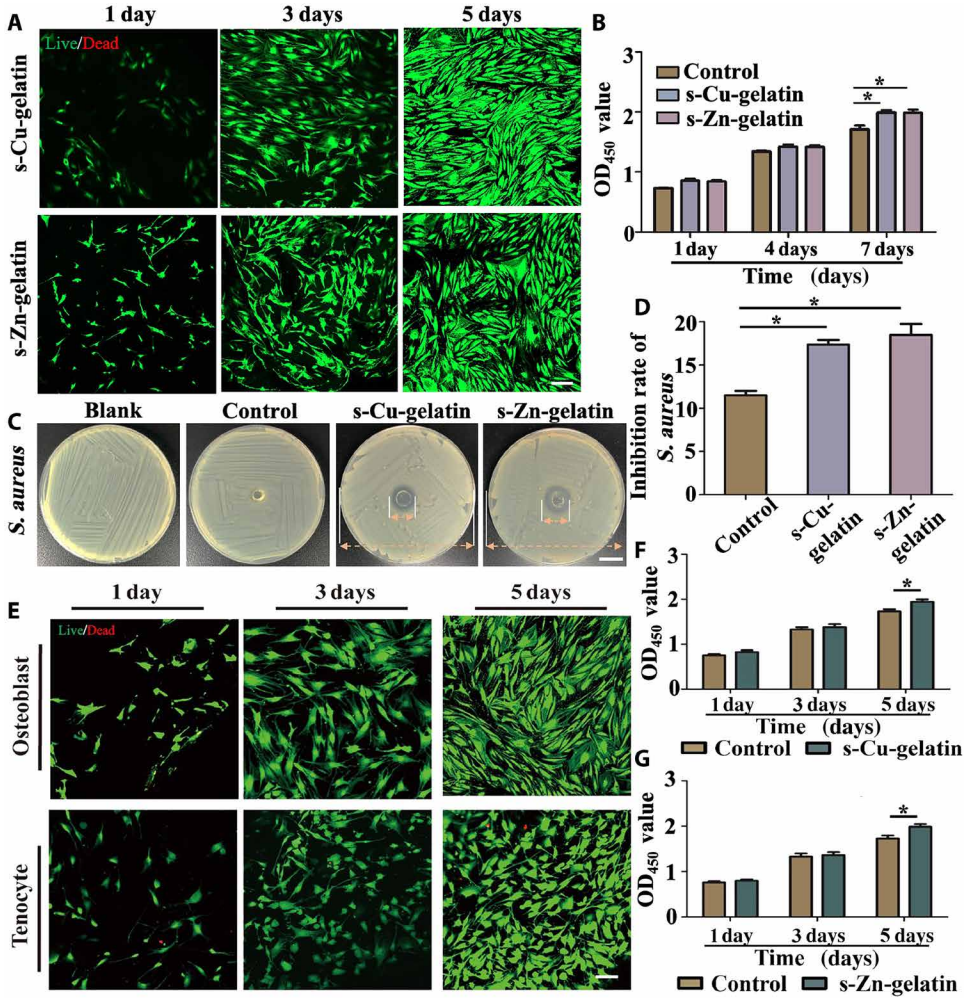

Fig. 3. Cytocompatibility and antibacterial properties of the gradient bimetallic hydrogel. (**A**) Representative fluorescence images showing live calcein-stained (green) and dead propidium iodide-labeled (red) rMSCs after culturing in s-Cu-gelatin and s-Zn-gelatin for 1, 3, and 5 days. Scale bar, 100 μm. (**B**) CCK8 assay showing the cell proliferation of cells after culturing for 1, 4, and 7 days ($n = 3$). (**C** and **D**) Antibacterial sensitivity of both gels against *S. aureus* based on the results of the agar diffusion test ($n = 3$). Scale bar, 1 cm. (**E**) Live/dead staining for osteoblasts and tenocytes after culturing in the novel hydrogel for 1, 3, and 5 days. (**F**) CCK8 assay showing osteoblast proliferation after culturing for 1, 4, and 7 days ($n = 3$). (**G**) CCK8 assay showing tenocyte proliferation after culturing for 1, 4, and 7 days ($n = 3$) (*$P < 0.05$). OD_{450}, optical density at 450 nm.

differentiation gradually increased over time (Fig. 5A). Furthermore, ALP activity was significantly higher in the s-Cu-gelatin group between days 3 and 7, compared to the s-gelatin group (Fig. 5B). Moreover, we also evaluated the mineralization activity to detect the osteogenic differentiation status on days 1, 7, 14, and 21, and the mineralized area of the cells increased gradually with time (Fig. 5C). After quantifying mineralization, it was determined that the s-Cu-gelatin group had denser mineral nodules and a higher degree of mineralization with statistical significance, compared to the s-gelatin group (Fig. 5D).

ALP and type I collagen (ColI) are early osteogenic markers (*35*, *36*). Runt-related transcription factor 2 (Runx2) is one of the most specific osteogenic differentiation markers in the early stage, whereas osteocalcin (OCN) is a late osteogenic marker (*37*, *38*). The gene expression of these markers was examined on different days. As shown in Fig. 5, (E to H), s-Cu-gelatin exhibited a powerful ability to promote the osteogenic differentiation of osteoblasts with statistical significance, compared to the s-gelatin.

Tenogenesis assay in vitro

We confirmed via flow cytometry that different concentrations (10^{-6} to 10^{-14} M) of zinc ions showed no influence on the viability of tenocytes (fig. S9). However, zinc ions at 10^{-8} and 10^{-12} M could significantly promote tenocyte proliferation after culturing for 3 days (Fig. 5I). Scleraxis (Scx) is the key transcriptional activator of tenocytes (*36*). As shown in Fig. 5F, the Scx protein expression in tenocytes was significantly up-regulated at 10^{-8} and 10^{-10} M zinc ions. The matrix metalloproteinase (MMP) family can degrade all ECM components of the tendon (*39*). However, the MMP13 protein expression did not significantly differ in tenocytes. Collagen protein contributed to maintaining the structure and strength of tendon tissue. ColI could provide stiff structures owing to its mechanical durability and strength, whereas ColIII was thinner than type I fibrils and was generally associated with scar tissue and injury (*40*, *41*). The expression of ColI protein in tenocytes was up-regulated at 10^{-8} and 10^{-10} M zinc ions, whereas that of ColIII protein was

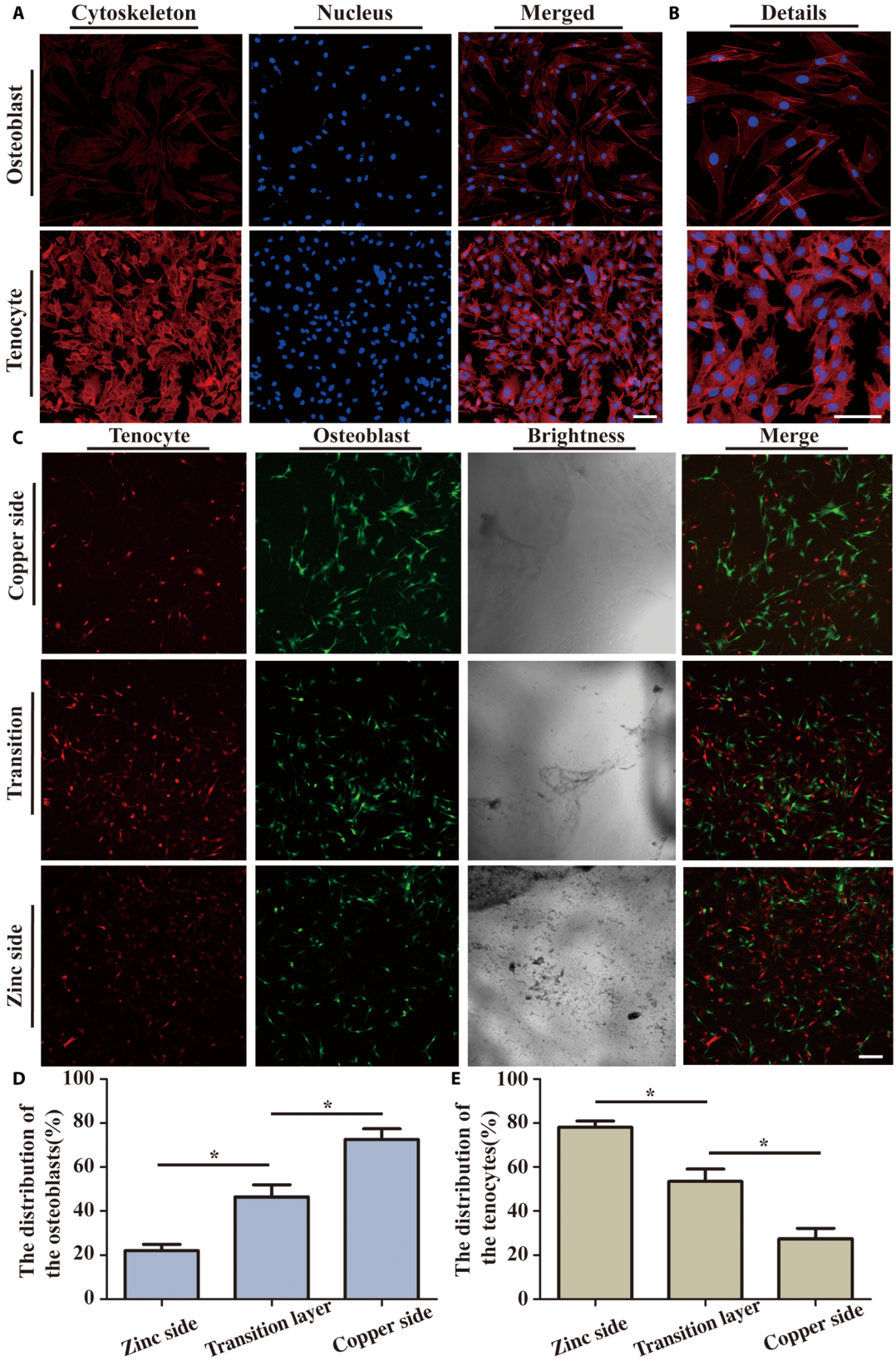

Fig. 4. In vitro assay of cell behavior. (**A**) Fluorescence images of cells double-stained with phalloidin for actin filaments (red) and DAPI for nuclei (blue) osteoblasts and tenocytes after culturing in bimetallic ion–based hydrogels for 3 days. (**B**) The details of the cytoskeleton. (**C**) The cell distribution on the different hydrogel surfaces. Scale bar, 100 μm. (**D** and **E**) Quantification of osteoblast and tenocyte distribution on the bimetallic hydrogels ($n = 3$) (*$P < 0.05$).

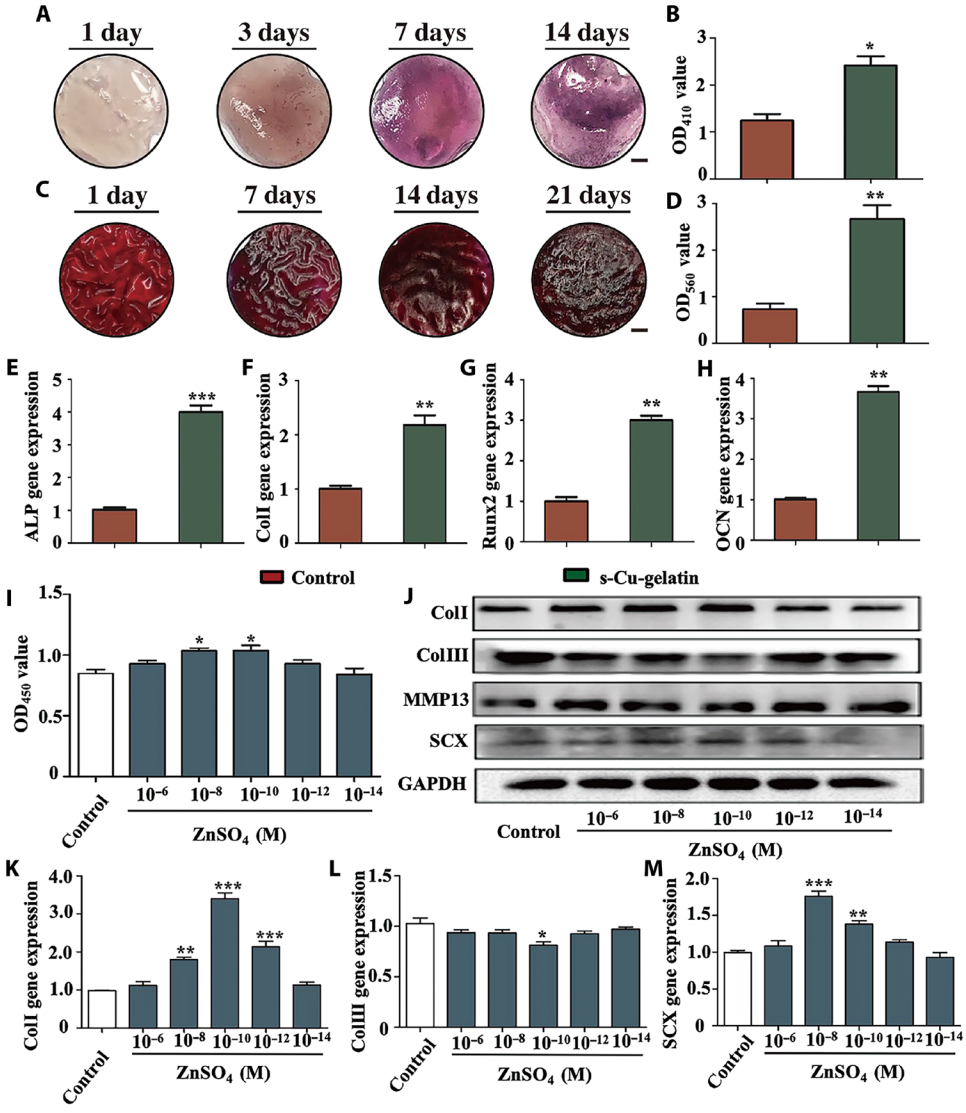

Fig. 5. In vitro assay of the effect on cell behavior. (**A**) ALP staining at days 1, 3, 7, and 14; representative images were shown. Scale bar, 2 mm. (**B**) Summarized data showing the ALP activity ($n = 3$). (**C**) The mineralized matrix was stained with ALP (Alizarin Red) at days 1, 7, 14, and 21; representative images were shown. Scale bar, 2 mm. (**D**) Summarized data showing the calcium production by quantifying the amount of Alizarin Red S that stained the mineralized matrix ($n = 3$). (**E** to **H**) The expression of osteogenesis-related genes, including Runx2, ColI, ALP after culturing for 7 days, and OCN after culturing for 14 days. (**I**) CCK8 assay showing the tenocyte proliferation after culturing for 3 days ($n = 3$). (**J**) ColI, ColIII, MMP13, SCX, and glyceraldehyde-3-phosphate dehydrogenase (GAPDH) protein expression levels in tenocytes stimulated by zinc ions. (**K** to **M**) The tendinous-related gene expressions in tenocytes stimulated by zinc ions, including ColI, ColIII, and SCX (n = 3) (*$P < 0.05$, **$P < 0.01$, and ***$P < 0.001$). Scale bars, 2 mm.

down-regulated at 10^{-8} and 10^{-10} M zinc (Fig. 5J). Moreover, the quantitative analysis of blots (fig. S11) indicated that the zinc ions had the ability to induce tenogenesis. The results of gene expression and protein expression were consistent. Notably, these results verified that zinc ions at some concentration (10^{-8} and 10^{-10} M) could promote tendon regeneration.

Evaluation of RCT regeneration efficacy in vivo

We translated our ion-based hydrogel to the in vivo RCT model of rats to evaluate tendon-to-bone interface regeneration. Moreover, the in vivo metabolism process was not consistent with the in vitro metabolism, and the in vivo synovial fluid is the viscous liquid in the synovial cavity and does not match the pure liquid environment. Therefore, we need to perform the in vivo experiment to confirm and complement the in vitro experiment results. After 4 and 8 weeks of recovery, the rats were examined using an animal magnetic resonance imaging (MRI) system and put the continuous sections to observe the newly formed tendon tissue in the rotator cuff (Fig. 6A and fig. S12). Then, they were sacrificed and examined via micro–computed tomography (CT) scanning to observe the newly formed bone (Fig. 6B and fig. S13). This is the first study to evaluate the healing effect on RCT via small-animal MRI. According to the results, the tendon regeneration status could be directly and visually evaluated. As shown in fig. S14, the direct observation of the microstructure revealed that the supraspinatus muscles were fuller and had better tension in the s-Cu/Zn-gelatin group compared with the

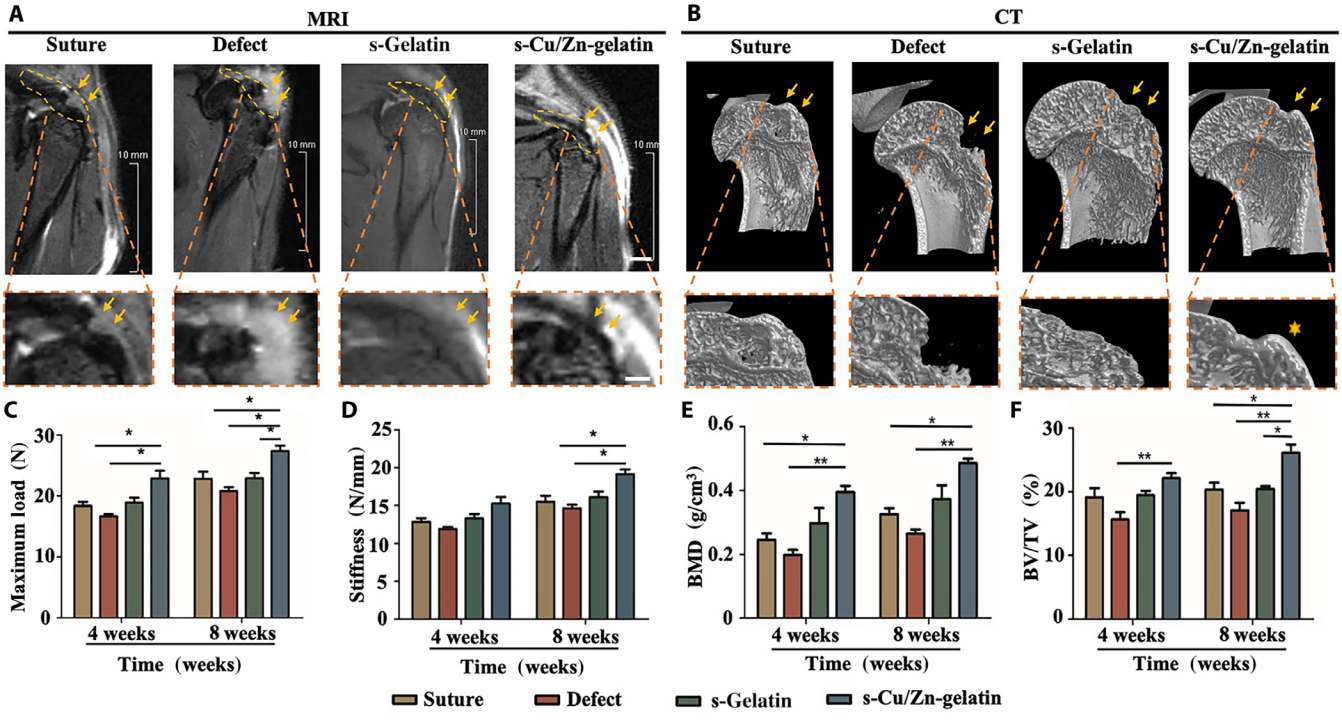

Fig. 6. The in vivo recovery capacity of the novel hydrogels. (**A**) After 8 weeks of implantation; representative images and MRI scanning images were taken to reveal the new tendon, highlighted in orange. Scale bar (general photo), 2mm; Scale bar (detail photo), 1mm. (**B**) The micro-CT images of different groups for 8 weeks. (**C** and **D**) The maximum load and stiffness values of the repaired rotator cuff tissue. (**E** and **F**) The bone volume density (BVD) and bone volume fraction (BV/YV) of the different groups ($n = 3$) (*$P < 0.05$, **$P < 0.01$).

other three groups. Moreover, the appearance and texture of tendons and muscles were not obviously different between the s-gelatin group and the pure suture group (suture group). But with regard to the tendon insert, the s-gelatin group showed more disorder, whereas the pure suture group had thinner and smaller areas. As for the defect group, the bone defect healed poorly, and an apparent defect was observed at the front of the tendon, making it stretch less. The MRI results were consistent with the general observed results, as shown in Fig. 6A. The tendons in the s-Cu/Zn-gelatin group had better tension, wider width, and a larger area of adhesion compared with the other three groups. The biomechanical experiments have confirmed the healing of the tendon-to-bone interface in the s-Cu/Zn-gelatin group (Fig. 6, C and D). Tension and toughness increased over time, as these were greater at 8 weeks than at 4 weeks. In addition, the maximum load and stiffness values of the s-Cu/Zn-gelatin groups were significantly higher than those of the other groups at weeks 4 and 8. No significant difference in maximum load values was observed between the s-gelatin mat group and the pure suture group (Fig. 6C). The stiffness values in the groups were not significantly different at week 4, and the s-Cu/Zn-gelatin mat group showed the highest value at week 8 (Fig. 6D). The suture and s-gelatin mat groups showed no significant differences in stiffness. Therefore, these results indicated better healing of the tendon tissue and tendon-to-bone interface in the s-Cu/Zn-gelatin group than in the other three groups.

Histological analysis

To observe the microstructure after recovery, we stained and analyzed the local tissue. By week 4, it was found that the repaired tendon failed to heal and immature granulation tissue with little collagen was present at the tendon-to-bone interface in all groups. Compared with the pure suture group, the s-gelatin mat and s-Cu/Zn-gelatin mat groups showed less infiltration by inflammatory cells as well as more regular morphology and arrangement of tendon tissue. By week 8, the repair process was completed gradually. Furthermore, the collagen fibers seemed to be more organized in the s-Cu/Zn-gelatin group than those in the other groups (Fig. 7A). According to the maturation scoring standards and compared with the pure suture and s-gelatin mat groups, the s-Cu/Zn-gelatin mat group showed a significant increase in tendon maturation ($P < 0.05$) at week 8 (Fig. 7B and Table 1) (*39*).

Toluidine blue staining was used to evaluate fibrocartilage in the tendon-to-bone section, as shown in Fig. 7C. The fibrocartilage area in the interface between the tendon and bone increased over time. Four weeks after surgery, the fibrocartilage showed a heterogeneous morphology and immature form, whereas after 8 weeks, the structure of the tissue appeared mature and complete with normal cell morphology and organizational structure. The fibrocartilage areas among the three groups were not statistically significant at week 4 (Fig. 7C). After 8 weeks, the fibrocartilage area was significantly larger in the s-Cu/Zn-gelatin mat group than in the suture repair and s-gelatin mat groups ($P < 0.05$) (Fig. 7D). The above results indicated that the s-Cu/Zn-gelatin mat is more favorable with respect to its ability to repair RCTs. In the process of fibrocartilage regeneration, cartilage regeneration and ingrowth were induced under the copper microenvironment, and tenocytes were recruited under the zinc microenvironment. Moreover, the different kinds of cells at both ends were affected by different ion microenvironments:

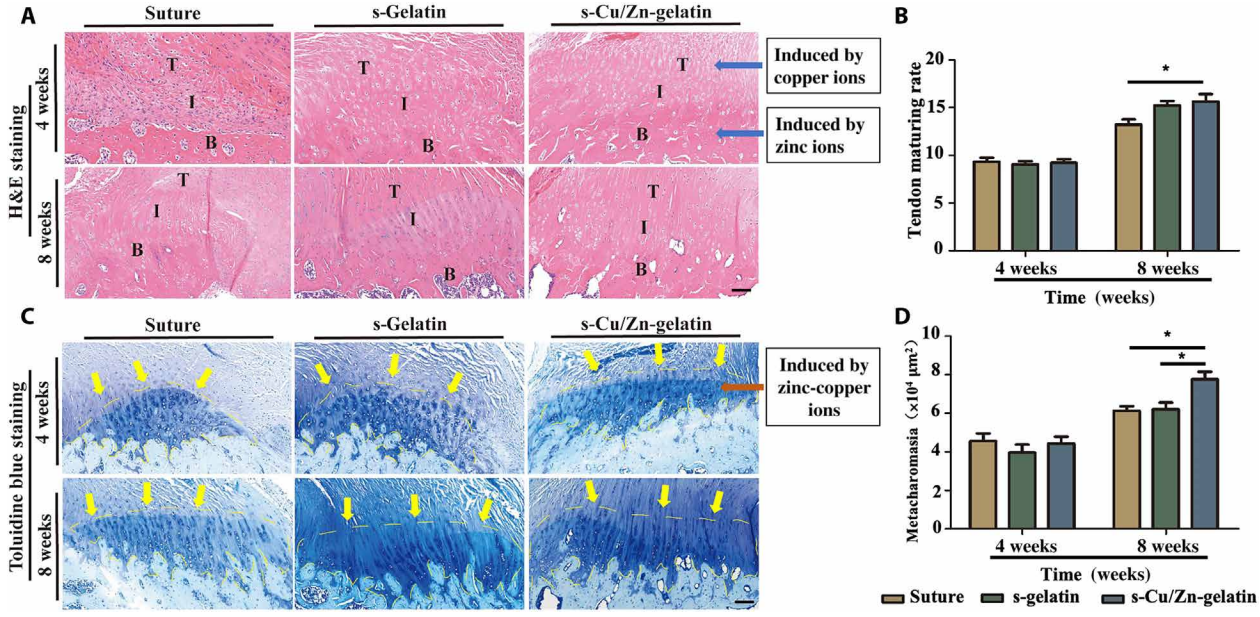

Fig. 7. Morphological analysis of the newly formed tendon-to-bone interface tissue after treatment. (**A**) Representative images of hematoxylin and eosin (H&E)–stained sections of mice treated with pure suture (suture), thiolation gelatin hydrogel (s-gelatin), and the bimetallic ion–based hydrogels (s-Cu/Zn-gelatin). T, tendon; I, interface; B, bone. (**B**) Tendon maturing score in the different treatment groups ($n = 3$). (**C**) Representative images of toluidine blue staining of mice with treatment. (**D**) The area of newly formed fibrocartilage in the different treatment groups ($n = 3$) (*$P < 0.05$). Scale bars, 100 μm.

Mineralization was induced in the tissue, whereas collagen secretion was promoted by tissue accumulation. Thus, differences in tissue ingrowth and the gradient mineralization process could promote synchronous fibrocartilage regeneration.

To evaluate the differential distribution and the organization of ColI and ColIII, picrosirius red staining was performed (*42*). As shown in fig. S15, the ColI in the repaired tendon of the s-Cu/Zn-gelatin groups was larger and more concentrated. Compared with the other two groups, the collagen fibers showed a more arranged distribution. These results demonstrated that the bimetallic ion–based hydrogels could promote collagen regeneration and alignment, which was beneficial for rotator cuff repair. Moreover, we have collected the rat's spleen, lung, and kidney after 2 months of the material implantation and performed tissue sectioning and hematoxylin and eosin (H&E) staining (fig. S16). Furthermore, no substantial harmful effect on the other tissues in the rat was observed after the implantation of the materials.

Table 1. The BMD and BV/TV values of the different groups.

	BMD		BV/TV	
	4 weeks	8 weeks	4 weeks	8 weeks
Suture	0.25 ± 0.04	0.33 ± 0.03	19.11 ± 2.53	20.34 ± 1.84
Defect	0.21 ± 0.02	0.26 ± 0.02	15.60 ± 2.05	17.06 ± 2.06
s-Gelatin	0.30 ± 0.08	0.37 ± 0.08	22.13 ± 1.35	20.43 ± 0.74
s-Cu/Zn-gelatin	0.39 ± 0.03	0.49 ± 0.03	22.13 ± 1.35	26.12 ± 2.24

DISCUSSION

In this study, the novel gradient bimetallic (Zn^{2+} and Cu^{2+}) ion–based hydrogel was fabricated, based on the principle of metal ion coordinate and cross-link thiolation gelatin. The results showed that this novel hydrogel system had greatly improved the method of healing acute full-thickness supraspinatus tendon rupture. Besides the functions of tissue repair, it also had the character of sustained release and antibacterial. This novel hydrogel induced good osteogenic differentiation and expression of tendon-related proteins, through the application in vitro. Furthermore, we demonstrated that this kind of material with bimetallic metal layers could promote fibrocartilage penetration by inducing bone and tendon repair simultaneously and effectively heal acute full-thickness supraspinatus tendon rupture.

Overall, the gradient microstructure plays an essential role in guiding the function of a wide range of tissues, including tendon, cartilage, and so on (*14*). The enthesis microstructure, such as the rotator cuff, is a typical gradient microstructure consisting of bones, mineralized fibrocartilage, unmineralized fibrocartilage, and tendons through gradations in structure. The challenge in the treatment of the RCT is the asynchronous regeneration of the tendon-bone interface, such as the incomplete regeneration of fibrocartilage interface and healing of vascularized scar tissue (*16*, *43*). Moreover, the poor healing of fibrocartilage in the tendon-to-bone interface could lead to poor functional outcomes and the re-tear. Therefore, the synchronous regeneration of gradient tissues is important for the complete regeneration of the RCT. At present, the proposed tissue engineering methods, such as electrospun fiber membranes and biomechanical patches that simulate the physiological structures (*23*, *44*), have several limitations, such as insufficient regeneration ability and poor biocompatibility. To solve the above problem, we propose a hydrogel system as the basic material that has the better cell affinity for tissue regeneration. Through the modification of gelatin with sulfhydryl groups, metal ions were added to the system

as cross-linking agents. We investigated the construction of gradient bimetal ion hydrogels and used the repairing properties of different metal ions. The ion gradient distribution in hydrogels induces the simultaneous regeneration of bone, tendon, and fibrocartilage tissue in the tendon-bone interface from different spatial levels, leading to the integrated repair and complete regeneration of the tendon-bone interface.

The EDS mapping was used to observe the ion gradient distribution in the constructed gradient bimetallic ion hydrogel. In our experiment, the EDS mapping is to count 250,000 U of elements in the horizontal plane through layer-by-layer scanning, so the porosity and uneven surface height lead to the lack of metal ions in the scan result area. But it could also be concluded that the Cu^{2+} and Zn^{2+} in the gradient section show the opposite transition trend. Almost one single metal ion distribution at the upper and lower layers and a mixed distribution of two ions at the intermediate interface were observed. Therefore, on the basis of the experimental results, it can be deduced that the gradient hydrogel was successfully constructed.

We then seeded different cells on the surface of the novel gradient hydrogel. On the basis of our findings, the gradient structure could arrange the ingrowth of osteoblasts under the copper microenvironment, and the tenocytes were recruited via the zinc microenvironment. This could be due to the fact that the different metal ions have different promoting effects on different cells. On the basis of our in vitro experiments, Cu^{2+} could have an effect on the proliferation and differentiation of osteoblasts, such as promoting proliferation and inducing the differentiation of osteoblasts. Similarly, Zn^{2+} could promote the proliferation of tenocytes and could also induce the expression of the tenogenesis-related gene of tendon cells. Therefore, the gradient metal ion hydrogel affects different cells at different corresponding positions. The above effect may contribute to the distribution in different cells.

Moreover, the different kinds of cells in both ends were affected by different ion microenvironments, the tissue in one end was induced to mineralization, and the tissue in the other end was accumulated to promote collagen secretion. Thus, the different tissue ingrowth and the gradient mineralization process could promote the fibrocartilage synchronous regeneration. Zinc deficiency would damage chondrocyte differentiation and increase apoptosis, and copper ions would considerably promote the proliferation and maturation of chondrocytes. This may be related to the joint involvement of Cu and Zn ions in the repair of fibrocartilage deactivation (*7*, *45*).

This study found that Zn^{2+} promoted the regeneration of tendon tissues. In addition, Zn^{2+} may promote tendon growth by activating the Smad2/3 and transforming growth factor–β (TGF-β) signaling pathways. Some researchers found that Zn^{2+} could activate the TGF-β pathway and up-regulate the expression of the Smad2/3 protein to promote the differentiation of cardiac progenitor cells (*46*). Moreover, the TGF-β and Smad2/3 signaling pathways are important for tendon cells to express SCX, which is the key transcription factor for tendon growth (*47*). Cu^{2+} plays an important role in angiogenesis. It could promote the tube formation of vascular endothelial cells by activating the hypoxia-inducible factor 1 (HIF-1) pathway and increase the expression of angiogenesis-related genes, such as vascular endothelial growth factor (*48*). HIF-1 is an important regulatory factor in the process of osteogenesis, which could regulate bone maturation and accelerate bone transformation (*49*). Therefore, Cu^{2+} may promote the osteogenic process by activating the HIF-1 pathway.

Fibrocartilage regeneration has always been the focus in the field of tendon-to-bone interface repair. In the present study, the metal ions have the tissue repair ability and the gradient arrangement of metal ions in the spatial structure of hydrogels that contributed to the repair of complex tissues. Tissue repair is possible due to the following:

1) Cu^{2+} could induce the overall repair of the osteochondral interface, whereas Zn^{2+} plays an important role in maintaining cartilage differentiation (*50*, *51*). Therefore, under the co-action of these two ions, it could promote cartilage regeneration and maintain the cartilage state in the transition layer area.

2) The difference between fibrocartilage and hyaline cartilage is that fibrocartilage has a large amount of fibrin. On the basis of the experimental results, both Cu^{2+} and Zn^{2+} could promote the expression of ColI in the corresponding cells, which was conducive to the arrangement of collagen in the fibrocartilage part and could promote the early formation of fibrocartilage.

3) In the tendon-bone interface, two kinds of fibrocartilage are present: mineralized fibrocartilage and nonmineralized fibrocartilage. On the basis of our experimental results, copper hydrogel has the ability to promote osteogenic differentiation, and zinc hydrogel has the ability to promote tendon differentiation. Moreover, in the area of the gradient structure of Cu/Zn ions, with the gradual increase of Cu^{2+}, the cells close to the high concentration layer of Cu^{2+} will gradually mineralize and evolve into mineralized fibrocartilage, whereas with the gradual increase of Zn^{2+}, the cells in the related area will maintain the appearance of fibrocartilage. The gradient arrangement of the metal ions was also the key reason for the formation of fibrocartilage.

4) The restoration of the early mechanical properties could also better promote the regeneration of fibrocartilage. Some researchers have proposed that a good mechanical environment could better promote the regeneration of fibrocartilage (*52*, *53*). On the basis of our in vivo experimental results, the mechanical properties in the s-Cu/Zn-gelatin groups, such as earlier tensile force and greater stiffness, are better than those of the other groups and provide a better mechanical environment to promote the regeneration of fibrocartilage. Therefore, the penetration of fibrocartilage may be induced by the metal ion gradient in the transition layer. The zinc ions present in the transition layer could promote collagen fiber penetration. The above processes may be the key to induce gradient formation resembling the locally physiological structure.

The healing effect of RCT was evaluated using small-animal MRI. The status of tendon regeneration could be directly and visually evaluated on the basis of the MRI imaging results. In clinics, MRI is an effective detection method to judge the integrity of soft tissue and fibrous connective tissue and the condition of the surrounding tissues (*54*). It can evaluate the rotator cuff from different spatial dimensions, such as sagittal, coronal, and oblique sagittal positions. In the present study, we provided three consecutive sagittal images to evaluate the rat rotator cuff tissue to judge the integrity and tension of the supraspinatus muscle from the front and back, so that the postoperative treatment effect could be more comprehensively evaluated. These imaging results are consistent with the results of the biomechanical strength and histological section that indicated better growth of the supraspinatus tendon and fibrocartilage in the tendon-to-bone interface.

Similarly, the MRI results could be matched with the general results of the postoperative rat. The dotted line marked the approximate

range of the supraspinatus muscle and the repair point of the tendon bone at the point of the arrow. In the simple suture group and the s-gelatin repair group, the surface fibers at the tendon-bone interface were chaotic. It was not completely repaired, with a noticeable tissue defect. While in the defect group, fibrous connection defects were observed. In the s-Cu/Zn-gelatin group, it was found that the fibers were more arranged, and the tissue at the tendon-bone junction was relatively complete. As for the MRI detection, the yellow dashed line roughly depicts the supraspinatus muscle tissue, and the yellow star marked the tendon-to-bone interface as shown in Fig. 6A. The black strips under the stars are the images of the supraspinatus muscle. In the simple suture group, the superior tendon has been connected to the greater tuberosity of the humerus, but a part of the tendon tissue on the surface has not yet been completely repaired. In the defect group, tendon tissue damage could be observed. In the s-gelatin group, the black strips were not tight and the whole tendinous tissue was swollen, indicating a rupture in the inner tendon and that it has not been completely repaired. In the s-Cu/Zn-gelatin group, it could be observed that the supraspinatus muscle was better attached to the bone surface, and the tendon bundle was relatively complete, which is consistent with the general observation results. Therefore, we concluded that the general results were consistent with the MRI results. This suggests that small-animal MRI could be used to diagnose RCT in rats.

According to the results of the animal experiments and tissue sections, the s-Cu/Zn-gelatin could promote the arrangement of collagen fibers in the tendon-bone interface. The possible reasons for this are as follows:

1) On the basis of the results of cell distribution, different types of cells are more likely to be distributed in the different areas of the material, tendon cells were more likely to be distributed on the surface of the s-Zn-gelatin hydrogel, and osteoblasts were more likely to be distributed on the surface of the s-Cu-gelatin hydrogel. With the early distribution of cells, both cells could better promote the secretion of collagen under the stimulation of the metal ions. Therefore, collagen fibers were secreted by the corresponding cells and distributed in the corresponding area, resulting in an anisotropic arrangement.

2) We believe that the heterogeneous arrangement of tissues could also be attributed to the early recovery of mechanical properties after surgery in the s-Cu/Zn-gelatin group. Clinically, the patient's postoperative recovery also requires rehabilitation methods to achieve the final complete recovery (*55*). On the basis of our results, the biomechanical properties of the tendon-to-bone tissue could be better restored under the induction of the gradient hydrogel, and it is more conducive to the arrangement of collagen under a good mechanical environment.

Aside from exploring the role of tissue regeneration and repair, we also conducted an in vitro antibacterial test. The target strain was *S. aureus*, which is the most common pathogen of infection that is present after rotator cuff injury and often causes postoperative shoulder pain, limited mobility, local fever, and swelling. When prolonged intravenous antibiotic treatment for postoperative shoulder joint infections, extensive soft tissue destruction, and tissue adhesion were prone to occur, it significantly reduces the postoperative functions (*56*). Therefore, a good tissue condition after surgery is conducive to tissue repair. According to the results of our study, gelatin did not have antibacterial properties, whereas Cu^{2+} and Zn^{2+} could be released from metal ion–based gelatin; the released metal ions exhibit the killing effect on *S. aureus* in the surrounding environment. Although the antibacterial experiment was the in vitro experiments, the principle of antibacterial capacity relied on the metal ions, which was released by hydrogels, and the ion-based hydrogel had a good release ability, so it could better simulate the internal environment. Moreover, on the basis of the results of the in vivo experiments, no shoulder joint infection was observed in the s-Cu/Zn-gelatin group after surgery, which could also prove that hydrogels have good antibacterial properties and could provide good physiological environmental conditions for postoperative repair.

The highly heterogeneous gradient material that simulates the structure of the tendon-to-bone interface was constructed in our study. This gradient material was used for the regeneration of tendon-to-bone interface that contains native tendon tissue. The novel structure of the materials had important roles:

1) The tendon-to-bone interface is the most important weight-bearing part in the body. It is the transition structure between the tendon tissue and the bone tissue and conducts the mechanical action between the two tissues. Many gradual factor evolutions include the change of composition (including ECM and cytokines) and the change of physiological properties (tissue stress and tissue morphological changes) (*14*). Thus, for the complete regeneration of this complex microstructure, the corresponding components cannot be supplemented alone.

It was necessary to use the spatial and repair characteristics of the material to achieve the synchronous repair of different tissues during the entire repair process. This is conducive to not only specific repairs for specific tissues but also the simultaneous integration of different tissues to achieve the overall homogeneity of cells, cytokines, and ECM between tissues after repair. Therefore, simulating the gradient structure of the tissue was beneficial to the synchronous regeneration of the complex tissue structure including the tendon and fibrocartilage.

2) In this study, we simulated the histological characteristics of the insertion site and suggested that the gradient hydrogel could be constructed by cross-linking the Cu^{2+} and Zn^{2+} with the sulfhydryl group to form a stable chelate, including the Zn^{2+} layer, Zn^{2+}/Cu^{2+} interface layer, and Cu^{2+} layer. On the basis of the biological effects at different spatial levels, these three different metal ion layers could achieve the synchronous healing of the different tissues in the tendon-bone interface.

The lastly released metal ions may be absorbed and metabolized by local tissues. The in vitro experiments have confirmed that the metal ion hydrogels, with a concentration of 0.05 M, had good biocompatibility, and this concentration of metal ions is always used to prepare bioactive hydrogels in the field of regenerative medicine (*57*, *58*).The results of the tissue morphology analysis after surgery, which included the liver, lung, and kidney, indicated that the implantation of hydrogel did not affect the tissue structure of these organs in the rat and showed that the released metal ions could be well metabolized by the body (fig. S16).

In summary, our study demonstrated the fabrication of gradient bimetallic ion–based hydrogels, which mimicked the physiological tissue gradient via the one-step coordinative cross-linking of sulfhydryl groups with copper and zinc ions for the microstructure reconstruction of the in situ tendon-to-bone insertion and had good mechanical strength, continuous slow-release properties, excellent biocompatibility, and antibacterial properties. This gradient bimetallic ion–based hydrogel system could induce tendon and bone

regeneration in RCT and promote the penetration of fibrocartilage into the tendon-to-bone insertion, in which the collagen fibers achieved better arrangement and biomechanics compared with the other groups. Therefore, these gradient bimetallic ion–based hydrogels may be used as a promising biomimetic biological material and provide a new treatment method to promote gradient microstructure healing.

MATERIALS AND METHODS

Fabrication of bimetallic ion–based hydrogels

First, thiol-gelatin powder (100 mg, 10 μmol theoretical thiols) was dissolved in 500μl of deionized water at 75°C to prepare a 20% s-gelatin hydrogel precursor. For gelation, the 500 μl of 0.05 M copper sulfate or zinc sulfate solution was mixed with the precursor solution and quickly poured into Teflon disc molds for 30 min at 37°C to generate the copper ion–based hydrogel (s-Cu-gelatin) and the zinc ion–based hydrogel (s-Zn-gelatin). In this way, the two kinds of the pregel solution stacked up and down at 75°C to generate the bimetallic ion–based hydrogels. All hydrogels were sterilized using ultraviolet light and alcohol and washed with PBS solution before using.

Characterization of bimetallic ion–based hydrogels

The surface morphological feature of the ion-based hydrogel was observed under SEM (Sirion 200) after treated with gold in an ion sputtering instrument for 45 s (SC7620, Quorum). The average pore diameter was calculated via the quantitative analysis of SEM images.

Moreover, 400 μl of ion-based hydrogel was used as samples for rheological study in oscillation mode with a 40-mm parallel plate. The frequency for strain sweep measurements was set at 10 rad/s. The strain for oscillation frequency measurements was set at 5%. The samples underwent a multistep process: 2% strain for 60 s, 200% strain for 60 s, 2% strain for 60 s, 200% strain for 60 s, and 2% strain for 60 s.

Ion release test was performed to determine the concentration of copper and zinc ions released from those gels. Overall, 200 μl of gels were prepared in a stereotype and immersed in 5 ml of 1× PBS inside of glass bottles. The bottles were incubated at a 37°C in a table concentrator. At certain time intervals (1, 3, 5, 7, 14, and 21 days), the whole solution in which the samples were immersed was diluted at a ratio of 4:1 with PBS solution and analyzed using a spectrometer (Optima 2100 DV, PerkinElmer). The test was performed on three independently prepared samples, and the results were presented as means ± SEM.

The weighed hydrogel was conducted in a 2-ml tube containing 1 ml of PBS or 1 ml of 0.15% collagenase type I solution shaken at 60 rpm at 37°C, respectively. The primary weight of gels was recorded as W_0. The weight of the remaining hydrogel that was recorded as W_t was calculated at different time points to calculate the degradation rate: Degradation rate (%) = $(W_0 - W_t)/W_0 \times 100\%$.

Cell viability and proliferation assay

Gels that undertook the aseptic processing with a total volume of 50 μl were prepared in 96-well plates and soaked in PBS solution at room temperature for 24 hours before cells contact with each other. Each well was seeded with 1×10^4 cells in α–minimum essential medium and incubated at 37°C with 5% CO_2; the medium was regularly changed for 1, 3, and 5 days. Then, the original medium was discarded, and the medium containing 10% CCK8 (Dojindo, Japan) was added and incubated for 1 hour. Subsequently, the 100-μl supernatant of each well was transferred to a new 96-well plate and detected at the 450-nm absorbance using a microplate reader (Model 680, Bio-Rad, USA). This test was performed in triplicates on three independently prepared samples, and the results were presented as means ± SD.

Flow cytometric analysis for apoptosis

The cells were seeded in a six-well plate (1×10^5 cells per well) after culturing for 24 hours and were treated with different concentrations of zinc sulfate solution for 24 hours. Then, cell apoptosis was examined using the FITC Annexin V Apoptosis Detection Kit (BD Biosciences, San Jose, CA, USA) in accordance with the manufacturer's instructions. The fluorescence intensity was measured using a Becton-Dickinson FACSCalibur flow cytometer (BD Biosciences).

Antibacterial activity of the hydrogels

The susceptibility of *S. aureus* to s-gelatin, s-Cu-gelatin, and s-Zn-gelatin hydrogels was determined by methods similar to the Kirby-Bauer disk diffusion test (Oxoid, United Kingdom). Briefly, 100 μl of s-gelatin solution is mixed with or without 100 μl of 0.05 M copper or zinc solution to form hydrogel. *S. aureus* was planted on the Mueller-Hinton agar plate (MH plate) using a cotton swab, and different kinds of hydrogels were planted on the center of the MH plate. Moreover, the *S. aureus* planted in the MH plate without any intervene was labeled as blank control. All of the groups were incubated at 37°C with 5% CO_2 for 48 hours. After the culture, the results were calculated and photographed, the approximate diameter of the antibacterial cycle was measured, and the statistical analysis was conducted according to the measured results.

Surgical procedure of rat RCT model

The rat RCT model was created to evaluate the repair ability of the ion-based hydrogel in vivo. In this study, a total of 48 Sprague-Dawley rats were used and randomly divided into four groups: gradient bimetallic ion–based hydrogel group (named as s-Cu/Zn-gelatin), pure thiol-gelatin group (named as s-gelatin), defect group (named as defect), and pure suture group (named as suture). The surgical procedure was roughly as follows: The animals were first ventilated with isoflurane, and their skin was partially disinfected to expose the deltoid muscle. Then, the deltoid muscle was cut, the supraspinatus muscle was exposed, and the supraspinatus muscle was isolated along the junction of the supraspinatus and the tibia. The 7# angle needle was used to drill the tunnel at the great nodule of the humerus, and the supraspinatus muscle was restitched to the large nodule using the 5# line, which can be stuffed into the material. Last, the rotator cuff injury model was completed. All animal experiments and breeding sites were provided by the Animal House of the Shanghai Institute of Trauma and Orthopedics. All experiments were in accordance with the animal welfare agreement.

Histopathological observation

On the day of sacrifice at weeks 4 and 8, the undecalcified samples of each group were fixed with 4% neutral formaldehyde buffer solution. After graded dehydration through an ethanol series, the samples were soaked in purified methyl methacrylate following sufficient infiltration and polymerization for nearly 60 days. Then, the well-embedded samples were longitudinally cut with a thickness of approximately 50 μm (Leica SP1600 cutting equipment, Germany). The sections were stained with toluidine blue to analyze the morphological changes of the newly formed bone tissues in the defect

sites. Moreover, the sections were labeled with picrosirius red stain to observe the types and distribution of the new collagen. The sections were then stained with H&E to evaluate the maturity of the new rotator cuff. The images were captured and recorded using confocal laser scanning microscopy (Leica TCS SP2, Germany).

Western blot analysis and quantitative real-time PCR analysis

The osteoblasts were subjected to different treatments, washed with PBS solution, homogenized with radioimmunoprecipiation assay lysis buffer blended with protease and phosphatase inhibitors at 4°C for 30 min, and shattered by ultrasound. Then, the cell extracts were centrifuged, and the supernatants were collected. The supernatant total protein was quantified using the Branford protein assay kit (KeyGen Biotech, Nanjing, China). The total protein was separated by SDS–polyacrylamide gel electrophoresis and then transferred onto the polyvinylidene difluoride membranes; the membranes were blocked for 1 hour in 5% skim milk diluted with tris-buffered saline containing 0.1% Tween 20 (TBST), followed by the incubation with primary antibodies overnight at 4°C. The membranes were washed with TBST and then incubated with horseradish peroxidase–conjugated secondary antibody for 1 hour at room temperature. The immune complex images were developed by enhanced chemiluminescence in the dark and were detected using a fluorescence imaging analysis system. The quantification of protein expression was performed via the ImageJ software (National Institutes of Health).

The total RNA was extracted using the TRIzol reagent and RNeasy Mini Kit. Overall, 500 ng of total RNA was reversely transcribed to cDNA using a cDNA transcription kit (Invitrogen). Quantitative real-time polymerase chain reaction (PCR) was performed using the LightCycler 480 PCR (Indianapolis, IN) with a 20-μl SYBR Green reaction system. PCR amplification was performed for 50 cycles. The expression of the housekeeping gene [glyceraldehyde-3-phosphate dehydrogenase (GAPDH)] was used to normalize gene expression levels.

Statistical analysis

The results of the experiments were statistically analyzed using the Statistical Package for the Social Sciences (SPSS) software (version 19.0). All data were presented as means ± SEM. Student's *t* tests (two-tailed unless otherwise stated) were performed for the comparison of two groups. One-way analysis of variance (ANOVA) was used for the analysis of three or more experimental groups. One-way ANOVA followed by Tukey's test was performed to assess the statistical difference using the SPSS software. The statistical tests conducted in this study are indicated in the figure legends as follows: $^{*}P < 0.05$, $^{**}P < 0.01$, and $^{***}P < 0.001$. The independent experiments ($n = 3$) were performed to guarantee the reproducibility of the findings.

SUPPLEMENTARY MATERIALS

Supplementary material for this article is available at http://advances.sciencemag.org/cgi/content/full/7/26/eabg3816/DC1

View/request a protocol for this paper from *Bio-protocol*.

REFERENCES AND NOTES

1. G. J. Anderson, D. M. Frazer, Current understanding of iron homeostasis. *Am. J. Clin. Nutr.* **106**, 1559S–1566S (2017).
2. J. H. de Baaij, J. G. Hoenderop, R. J. Bindels, Magnesium in man: Implications for health and disease. *Physiol. Rev.* **95**, 1–46 (2015).
3. P. H. Lin, M. Sermersheim, H. Li, P. H. U. Lee, S. M. Steinberg, J. Ma, Zinc in wound healing modulation. *Nutrients* **10**, 16 (2017).
4. P. Wychowanski, K. Malkiewicz, Evaluation of metal ion concentration in hard tissues of teeth in residents of central Poland. *Biomed. Res. Int.* **2017**, 6419709 (2017).
5. C. Wu, Y. Zhou, M. Xu, P. Han, L. Chen, J. Chang, Y. Xiao, Copper-containing mesoporous bioactive glass scaffolds with multifunctional properties of angiogenesis capacity, osteostimulation and antibacterial activity. *Biomaterials* **34**, 422–433 (2013).
6. A. Yousefi, F. Sarrafzadeh-Rezaei, S. Asri-Rezaei, A. A. Farshid, M. Behfar, Fabrication of novel tubular scaffold for tendon repair from chitosan in combination with zinc oxide nanoparticles. *Vet Res Forum* **9**, 105–111 (2018).
7. R. Lin, C. Deng, X. Li, Y. Liu, M. Zhang, C. Qin, Q. Yao, L. Wang, C. Wu, Copper-incorporated bioactive glass-ceramics inducing anti-inflammatory phenotype and regeneration of cartilage/bone interface. *Theranostics* **9**, 6300–6313 (2019).
8. M. S. Rashid, C. Cooper, J. Cook, D. Cooper, S. G. Dakin, S. Snelling, A. J. Carr, Increasing age and tear size reduce rotator cuff repair healing rate at 1 year. *Acta Orthop.* **88**, 606–611 (2017).
9. F. Oliva, L. Osti, J. Padulo, N. Maffulli, Epidemiology of the rotator cuff tears: A new incidence related to thyroid disease. *Muscles Ligaments Tendons J* **4**, 309–314 (2014).
10. R. I. Sharma, J. G. Snedeker, Biochemical and biomechanical gradients for directed bone marrow stromal cell differentiation toward tendon and bone. *Biomaterials* **31**, 7695–7704 (2010).
11. A. C. Deymier-Black, J. D. Pasteris, G. M. Genin, S. Thomopoulos, Allometry of the tendon enthesis: Mechanisms of load transfer between tendon and bone. *J. Biomech. Eng.* **137**, 111005 (2015).
12. L. Rossetti, L. A. Kuntz, E. Kunold, J. Schock, K. W. Muller, H. Grabmayr, J. Stolberg-Stolberg, F. Pfeiffer, S. A. Sieber, R. Burgkart, A. R. Bausch, The microstructure and micromechanics of the tendon-bone insertion. *Nat. Mater.* **16**, 664–670 (2017).
13. S. Patel, A. P. Gualtieri, H. H. Lu, W. N. Levine, Advances in biologic augmentation for rotator cuff repair. *Ann. N. Y. Acad. Sci.* **1383**, 97–114 (2016).
14. C. Li, L. Ouyang, I. J. Pence, A. C. Moore, Y. Lin, C. W. Winter, J. P. K. Armstrong, M. M. Stevens, Buoyancy-driven gradients for biomaterial fabrication and tissue engineering. *Adv. Mater.* **31**, e1900291 (2019).
15. H. H. Lu, S. Thomopoulos, Functional attachment of soft tissues to bone: Development, healing, and tissue engineering. *Annu. Rev. Biomed. Eng.* **15**, 201–226 (2013).
16. C. Zhu, S. Pongkitwitoon, J. Qiu, S. Thomopoulos, Y. Xia, Design and fabrication of a hierarchically structured scaffold for tendon-to-bone repair. *Adv. Mater.* **30**, e1707306 (2018).
17. J. A. Neumann, M. H. Zgonis, K. D. Rickert, K. E. Bradley, T. J. Kremen, B. R. Boggess, A. P. Toth, Interposition dermal matrix xenografts: A successful alternative to traditional treatment of massive rotator cuff tears. *Am. J. Sports Med.* **45**, 1261–1268 (2017).
18. A. K. Gupta, K. Hug, D. J. Berkoff, B. R. Boggess, M. Gavigan, P. C. Malley, A. P. Toth, Dermal tissue allograft for the repair of massive irreparable rotator cuff tears. *Am. J. Sports Med.* **40**, 141–147 (2012).
19. D. F. E. Ker, D. Wang, A. W. Behn, E. T. H. Wang, X. Zhang, B. Y. Zhou, A. E. Mercado-Pagan, S. Kim, J. Kleimeyer, B. Gharaibeh, Y. Shanjani, D. Nelson, M. Safran, E. Cheung, P. Campbell, Y. P. Yang, Functionally graded, bone- and tendon-like polyurethane for rotator cuff repair. *Adv. Funct. Mater.* **28**, 1707107 (2018).
20. Q. Liu, Y. Yu, R. L. Reisdorf, J. Qi, C. K. Lu, L. J. Berglund, P. C. Amadio, S. L. Moran, S. P. Steinmann, K. N. An, A. Gingery, C. Zhao, Engineered tendon-fibrocartilage-bone composite and bone marrow-derived mesenchymal stem cell sheet augmentation promotes rotator cuff healing in a non-weight-bearing canine model. *Biomaterials* **192**, 189–198 (2019).
21. M. J. Smith, J. L. Cook, K. Kuroki, P. S. Jayabalan, C. R. Cook, F. M. Pfeiffer, N. P. Waters, Comparison of a novel bone-tendon allograft with a human dermis-derived patch for repair of chronic large rotator cuff tears using a canine model. *Art Ther.* **28**, 169–177 (2012).
22. T. Thangarajah, C. J. Pendegrass, S. Shahbazi, S. Lambert, S. Alexander, G. W. Blunn, Augmentation of rotator cuff repair with soft tissue scaffolds. *Orthop. J. Sports Med.* **3**, 2325967115587495 (2015).
23. X. Li, R. Cheng, Z. Sun, W. Su, G. Pan, S. Zhao, J. Zhao, W. Cui, Flexible bipolar nanofibrous membranes for improving gradient microstructure in tendon-to-bone healing. *Acta Biomater.* **61**, 204–216 (2017).
24. L. Wang, C. Hu, L. Shao, The antimicrobial activity of nanoparticles: Present situation and prospects for the future. *Int. J. Nanomedicine* **12**, 1227–1249 (2017).
25. A. Ewald, C. Kappel, E. Vorndran, C. Moseke, M. Gelinsky, U. Gbureck, The effect of Cu(II)-loaded brushite scaffolds on growth and activity of osteoblastic cells. *J. Biomed. Mater. Res. A* **100**, 2392–2400 (2012).
26. H. Geckil, F. Xu, X. Zhang, S. Moon, U. Demirci, Engineering hydrogels as extracellular matrix mimics. *Nanomedicine (Lond.)* **5**, 469–484 (2010).
27. M. Rosenberg, H. Vija, A. Kahru, C. W. Keevil, A. Ivask, Rapid in situ assessment of Cu-ion mediated effects and antibacterial efficacy of copper surfaces. *Sci. Rep.* **8**, 8172 (2018).
28. M. C. Echave, L. Saenz del Burgo, J. L. Pedraz, G. Orive, Gelatin as biomaterial for tissue engineering. *Curr. Pharm. Des.* **23**, 3567–3584 (2017).
29. K. De Clercq, C. Schelfhout, M. Bracke, O. De Wever, M. Van Bockstal, W. Ceelen, J. P. Remon, C. Vervaet, Genipin-crosslinked gelatin microspheres as a strategy to prevent postsurgical peritoneal adhesions: In vitro and in vivo characterization. *Biomaterials* **96**, 33–46 (2016).

30. Q. Saiding, J. Jin, M. Qin, Z. Cai, M. Lu, F. Wang, W. Cui, X. Chen, Heat-shrinkable electrospun fibrous tape for restoring structure and function of loose soft tissue. *Adv. Funct. Mater.* **31**, 2007440 (2021).
31. P. Kaali, M. M. Perez-Madrigal, E. Stromberg, R. E. Aune, G. Czel, S. Karlsson, The influence of Ag^{+}, Zn^{2+} and Cu^{2+} exchanged zeolite on antimicrobial and long term in vitro stability of medical grade polyether polyurethane. *Express Polym Lett* **5**, 1028–1040 (2011).
32. A. Trampuz, W. Zimmerli, Diagnosis and treatment of infections associated with fracture-fixation devices. *Injury* **37** (Suppl 2), S59–S66 (2006).
33. W. J. Metsemakers, R. Kuehl, T. F. Moriarty, R. G. Richards, M. H. J. Verhofstad, O. Borens, S. Kates, M. Morgenstern, Infection after fracture fixation: Current surgical and microbiological concepts. *Injury* **49**, 511–522 (2018).
34. A. Prasad, E. Alizadeh, Cell form and function: Interpreting and controlling the shape of adherent cells. *Trends Biotechnol.* **37**, 347–357 (2019).
35. E. Wrobel, J. Leszczynska, E. Brzoska, The characteristics of human bone-derived cells (HBDCS) during osteogenesis in vitro. *Cell. Mol. Biol. Lett.* **21**, 26 (2016).
36. M. Rezai Rad, M. Bohloli, M. Akhavan Rahnama, A. Anbarlou, P. Nazeman, A. Khojasteh, Impact of tissue harvesting sites on the cellular behaviors of adipose-derived stem cells: Implication for bone tissue engineering. *Stem Cells Int* **2017**, 2156478 (2017).
37. J. Xu, Z. Li, Y. Hou, W. Fang, Potential mechanisms underlying the Runx2 induced osteogenesis of bone marrow mesenchymal stem cells. *Am J Transl Res* **7**, 2527–2535 (2015).
38. J. Cao, Y. Wei, J. Lian, L. Yang, X. Zhang, J. Xie, Q. Liu, J. Luo, B. He, M. Tang, Notch signaling pathway promotes osteogenic differentiation of mesenchymal stem cells by enhancing BMP9/Smad signaling. *Int. J. Mol. Med.* **40**, 378–388 (2017).
39. S. Minkwitz, A. Schmock, A. Kurtoglu, S. Tsitsilonis, S. Manegold, B. Wildemann, F. Klatte-Schulz, Time-dependent alterations of MMPs, TIMPs and tendon structure in human achilles tendons after acute rupture. *Int. J. Mol. Sci.* **18**, 2199 (2017).
40. M. R. Buckley, E. B. Evans, P. E. Matuszewski, Y. L. Chen, L. N. Satchel, D. M. Elliott, L. J. Soslowsky, G. R. Dodge, Distributions of types I, II and III collagen by region in the human supraspinatus tendon. *Connect. Tissue Res.* **54**, 374–379 (2013).
41. H. J. Stark, M. J. Willhauck, N. Mirancea, K. Boehnke, I. Nord, D. Breitkreutz, A. Pavesio, P. Boukamp, N. E. Fusenig, Authentic fibroblast matrix in dermal equivalents normalises epidermal histogenesis and dermoepidermal junction in organotypic co-culture. *Eur. J. Cell Biol.* **83**, 631–645 (2004).
42. N. Zerbinati, A. Calligaro, Calcium hydroxylapatite treatment of human skin: Evidence of collagen turnover through picrosirius red staining and circularly polarized microscopy. *Clin Cosmet Investig Dermatol* **11**, 29–35 (2018).
43. J. H. Oh, S. H. Kim, H. M. Ji, K. H. Jo, S. W. Bin, H. S. Gong, Prognostic factors affecting anatomic outcome of rotator cuff repair and correlation with functional outcome. *Art Ther.* **25**, 30–39 (2009).
44. T. W. Qin, Y. L. Sun, A. R. Thoreson, S. P. Steinmann, P. C. Amadio, K. N. An, C. Zhao, Effect of mechanical stimulation on bone marrow stromal cell-seeded tendon slice constructs: A potential engineered tendon patch for rotator cuff repair. *Biomaterials* **51**, 43–50 (2015).
45. G. Murphy, M. H. Lee, What are the roles of metalloproteinases in cartilage and bone damage? *Ann. Rheum. Dis.* **64**, iv44–iv47 (2005).
46. T. Huang, E. J. Ditzel, A. B. Perrera, D. M. Broka, T. D. Camenisch, Arsenite disrupts zinc-dependent TGFβ2-SMAD activity during murine cardiac progenitor cell differentiation. *Toxicol. Sci.* **148**, 409–420 (2015).
47. T. Maeda, T. Sakabe, A. Sunaga, K. Sakai, A. L. Rivera, D. R. Keene, T. Sasaki, E. Stavnezer, J. Iannotti, R. Schweitzer, D. Ilic, H. Baskaran, T. Sakai, Conversion of mechanical force into TGF-β-mediated biochemical signals. *Curr. Biol.* **21**, 933–941 (2011).
48. Z. Zhang, L. Qiu, C. Lin, H. Yang, H. Fu, R. Li, Y. J. Kang, Copper-dependent and -independent hypoxia-inducible factor-1 regulation of gene expression. *Metallomics* **6**, 1889–1893 (2014).
49. J. Shao, Y. Zhang, T. Yang, J. Qi, L. Zhang, L. Deng, HIF-1α disturbs osteoblasts and osteoclasts coupling in bone remodeling by up-regulating OPG expression. *In Vitro Cell. Dev. Biol. Anim.* **51**, 808–814 (2015).
50. C. Xu, J. Chen, L. Li, X. Pu, X. Chu, X. Wang, M. Li, Y. Lu, X. Zheng, Promotion of chondrogenic differentiation of mesenchymal stem cells by copper: Implications for new cartilage repair biomaterials. *Korean J. Couns. Psychother.* **93**, 106–114 (2018).
51. T. C. Huang, W. T. Chang, Y. C. Hu, B. S. Hsieh, H. L. Cheng, J. H. Yen, P. R. Chiu, K. L. Chang, Zinc protects articular chondrocytes through changes in Nrf2-mediated antioxidants, cytokines and matrix metalloproteinases. *Nutrients* **10**, 471 (2018).
52. S. Thomopoulos, R. Das, V. Birman, L. Smith, K. Ku, E. L. Elson, K. M. Pryse, J. P. Marquez, G. M. Genin, Fibrocartilage tissue engineering: The role of the stress environment on cell morphology and matrix expression. *Tissue Eng. Part A* **17**, 1039–1053 (2011).
53. X. Su, J. Wang, H. Kang, G. Bao, L. Liu, Effects of dynamic radial tensile stress on fibrocartilage differentiation of bone marrow mesenchymal stem cells. *Biomed. Eng. Online* **19**, 8 (2020).
54. Y. Xie, S. Liu, Y. Qiao, Y. Hu, Y. Zhang, J. Qu, Y. Shen, H. Tao, S. Chen, Quantitative T2 mapping-based tendon healing is related to the clinical outcomes during the first year after arthroscopic rotator cuff repair. *Knee Surg. Sports Traumatol. Arthrosc.* **29**, 127–135 (2021).
55. A. D. Kaye, R. D. Urman, E. M. Cornett, B. M. Hart, A. Chami, J. A. Gayle, C. J. Fox, Enhanced recovery pathways in orthopedic surgery. *J Anaesthesiol Clin Pharmacol* **35**, S35–S39 (2019).
56. K. Atesok, P. MacDonald, J. Leiter, S. McRae, G. Stranges, J. Old, Postoperative deep shoulder infections following rotator cuff repair. *World J. Orthop.* **8**, 612–618 (2017).
57. L. Cheng, Z. Cai, T. Ye, X. Yu, Z. Chen, Y. Yan, J. Qi, L. Wang, Z. Liu, W. Cui, L. Deng, Injectable polypeptide-protein hydrogels for promoting infected wound healing. *Adv. Funct. Mater.* **30**, 2001196 (2020).
58. M. Shahriari-Khalaji, S. Hong, G. Hu, Y. Ji, F. F. Hong, Bacterial nanocellulose-enhanced alginate double-network hydrogels cross-linked with six metal cations for antibacterial wound dressing. *Polymers* **12**, 1–20 (2020).

Acknowledgments

Funding: This study was financially supported by National Key Research and Development Program of China (2018YFC1106200), National Natural Science Foundation of China (81972134 and 81930051), Science and Technology Commission of Shanghai Municipality (19ZR1448000 and 18ZR1434200), Key Clinical Specialty Construction Program of Shanghai during the 13th Five-Year Plan period (shslczdzk04802), the Youth Science and Technology Innovation Studio of Shanghai Jiao Tong University School of Medicine (JYKCGZS01), and Shanghai Municipal Health Commission Health Industry Clinical Research Project (20204Y0351). **Author contributions:** R.Y., G.L., and C.Z. prepared materials, designed and performed research, analyzed the data, and wrote the manuscript; P.Y. prepared the materials and analyzed the data; T.Y. and Y.Z. performed the research in vitro; P.S., J.H., and M.C. performed the research in vivo; L.W. conceptualized and designed the research; W.C. outlined and edited the manuscript; and L.D. designed the research and provided the laboratory space and funding. **Competing interests:** The authors declare that they have no competing interests. **Data and materials availability:** All data needed to evaluate the conclusions in the paper are present in the paper and/or the Supplementary Materials. Additional data related to this paper may be requested from the authors.

Submitted 1 January 2021
Accepted 29 April 2021
Published 23 June 2021
10.1126/sciadv.abg3816

Citation: R. Yang, G. Li, C. Zhuang, P. Yu, T. Ye, Y. Zhang, P. Shang, J. Huang, M. Cai, L. Wang, W. Cui, L. Deng, Gradient bimetallic ion–based hydrogels for tissue microstructure reconstruction of tendon-to-bone insertion. *Sci. Adv.* **7**, eabg3816 (2021).

ScienceAdvances

Gradient bimetallic ion–based hydrogels for tissue microstructure reconstruction of tendon-to-bone insertion

Renhao Yang, Gen Li, Chengyu Zhuang, Pei Yu, Tingjun Ye, Yin Zhang, Peiyang Shang, Jingjing Huang, Ming Cai, Lei Wang, Wenguo Cui, and Lianfu Deng

Sci. Adv. **7** (26), eabg3816. DOI: 10.1126/sciadv.abg3816

Science Advances (ISSN 2375-2548) is published by the American Association for the Advancement of Science. 1200 New York Avenue NW, Washington, DC 20005. The title *Science Advances* is a registered trademark of AAAS.